A Detailed Kinetic Model for Biogas Steam Reforming on Ni and Catalyst Deactivation Due to Sulfur Poisoning

Srinivas Appari[a], Vinod M. Janardhanan[a,1], Ranjit Bauri[b], Sreenivas Jayanti[c], Olaf Deutschmann[d]

[a]*Department of Chemical Engineering, Indian Institute of Technology Hyderabad, Andhra Pradesh 502 205, India*
[b]*Department of Metallurgical and Materials Engineering, Indian Institute of Technology Madras, Chennai 600 036, Tamil Nadu, India*
[c]*Department of Chemical Engineering, Indian Institute of Technology Madras, Chennai 600 036, Tamil Nadu, India*
[d]*Institute for Chemical Technology and Polymer Chemistry, Karlsruhe Institute of Technology, Engesserstr. 20, 76131 Karlsruhe, Germany*

Abstract

This paper deals with the development and validation of a detailed kinetic model for steam reforming of biogas with and without H_2S. The model has 68 reactions among 8 gasphase species and 18 surface adsorbed species including the catalytic surface. The activation energies for various reactions are calculated based on unity bond index-quadratic exponential potential (UBI-QEP) method. The whole mechanism is made thermodynamically consistent by using a previously published algorithm. Sensitivity analysis is carried out to understand the influence of reaction parameters on surface coverage of sulfur. The parameters describing sticking and desorption reactions of H_2S are the most sensitive ones for the formation of adsorbed sulfur. The mechanism is validated in the temperature range of 873-1200 K for biogas free from H_2S and 973-1173 K for biogas containing 20-108 ppm H_2S. The model predicts that during the initial stages of poisoning sulfur coverages are high near the reactor inlet; however, as the reaction proceeds further sulfur coverages increase towards the reactor exit. In the absence of sulfur CO and H atoms are the dominant surface adsorbed species. High temperature operation can significantly mitigate sulfur adsorption and hence the saturation sulfur coverages are lower compared to low temperature operation. Low temperature operation can lead to full deactivation of the catalyst. The model predicts saturation coverages that are comparable to experimental observation.

Key words: Biogas, Reforming, Catalyst Poisoning, Kinetics, Deactivation, Modeling

1. Introduction

Biogas is an important source of renewable energy produced by the anaerobic digestion of biomass. The composition of biogas depends on the biomass source and duration of digestion process. Generally it contains 50-75% CH_4, 50-25% CO_2, 0-10% N_2, and 0-3% H_2S. Biogas may be combusted to produce electricity or can be converted to synthesis gas by reforming over Rh or Ni catalyst [1, 2, 3, 4]. However, the presence of H_2S or other sulfur containing compounds is a major problem for reforming of biogas due to its poisoning effect on most transition metals [5]. Although poisoning of Ni in presence of H_2S is well known, the mechanistic details of poisoning and regeneration are lacking in the present literature, particularly in biogas environment. The blocking of active catalytic sites is the root cause for poisoning. In general poisoning effect varies exponentially with time on stream and the final activity of the catalyst depends on the uncovered active surface available. The saturation coverage of sulfur and other species depends on the operating temperature, metal loading, and the partial pressure of reacting gases. Catalysts with lower metal loading lose activity at a faster rate compared to catalysts with higher metal loading [6]. Essentially for low metal loading the sulfur adsorption capacity is lower due to the low surface area.

The chemisorption of sulfur on Ni is a reversible process [7]. Therefore, exposing it to appropriate operating conditions can regenerate the sulfur deactivated Ni catalyst. Removal of H_2S from the feed gas can recover the catalyst activity or in other words lower H_2S concentrations in the feed gas leads to lesser extend of poisoning. Since chemisorption is an exothermic process, adsorbed sulfur can be removed by increasing the temperature [8]. Therefore, for any given H_2S partial pressure, high temperature operation leads to low activity loss. Based on the available information in literature and our own experiments this work develops a detailed kinetic model for poisoning of Ni catalyst during biogas reforming. There are several review articles outlining various aspects of catalyst poisoning [9, 10], however, models that deal with catalyst poisoning are really scarce in literature. The general practice in modeling catalyst poisoning is to express the activity, i.e the ratio of true rate to the initial rate, as a function of time and poison concentration [11, 12, 13, 14]. This work appears to be the first attempt to model sulfur poisoning on Ni catalyst using a detailed kinetic model. The root of the kinetic model is a previously published mechanism for steam reforming of CH_4 on Ni [15]. Additional reactions are incorporated into this mechanism to account for sulfur adsorption, desorption, disproportionation, and recombination reactions. The activation energies for the elementary step reactions are calculated by UBI-QEP method [16]. The developed kinetic model is

Email address: vj@iith.ac.in (Vinod M. Janardhanan)

validated by comparing the model predictions with our own experiments and the experiments reported by other research groups [3, 17, 18]. These experiments were performed in isothermal fixed bed reactors. Therefore, a one dimensional fixed bed reactor model is used to simulate the experiments.

2. Reactor model

A one-dimensional transient fixed bed reactor model is used for the simulations presented in this work. Assuming ideal gas behavior and constant pressure, the partial differential equation that describes the species transport in a fixed bed reactor with constant mass flow rate is:

$$\rho\frac{\partial Y_k}{\partial t} = -\dot{m}\frac{\partial Y_k}{\partial x} + \frac{\partial}{\partial x}\left(\mathcal{D}^{\mathrm{e}}_{\mathrm{km}}\frac{\partial \rho Y_k}{\partial x}\right) + A_{\mathrm{v}} W_k \dot{s}_k, \quad k = 1, \ldots, N_{\mathrm{g}} \tag{1}$$

Here, ρ is the density, Y_k is the mass fraction of species k, t is the time, $\dot{m}$ is the mass flux, $\mathcal{D}^{\mathrm{e}}_{\mathrm{km}}$ is the effective diffusion coefficient of species k in the mixture, A_{v} is the active area available for chemical reactions per unit volume, $\dot{s}_k$ is the molar production rate of gasphase species k, W_k is the molecular weight of species k, N_{g} is the number of gasphase species, and x is the axial coordinate. The density ρ is calculated from the ideal gas equation:

$$p\bar{M} = \rho R T, \tag{2}$$

where $\bar{M}$ is the average molecular weight, R is the gas constant, and T is the temperature. The effective diffusion coefficient is defined as

$$\mathcal{D}^{\mathrm{e}}_{\mathrm{km}} = \frac{\epsilon}{\tau}\mathcal{D}_{\mathrm{km}}, \tag{3}$$

where ϵ is the porosity and τ is the tortuosity of porous pellets. The mixture diffusion coefficient of species k in the mixture $\mathcal{D}_{\mathrm{km}}$ is calculated according to

$$\mathcal{D}_{\mathrm{km}} = \frac{1 - Y_k}{\sum_{j\neq k}^{N_{\mathrm{g}}} X_j/\mathcal{D}_{\mathrm{jk}}}. \tag{4}$$

Here X_j is the mole fraction of species j, and the binary diffusion coefficient $\mathcal{D}_{\mathrm{jk}}$ is calculated according to Chapman-Enskog theory [19]. Since the catalyst poisoning is mainly due to loss in active surface area A_{v} is not a constant and changes with sulfur coverage. In the present calculations, we assume a linear dependence of A_{v} on the sulfur coverage [20]. i.e.,

$$A_{\mathrm{v}} = A_{\mathrm{v0}}(1 - \theta_{\mathrm{s}}), \tag{5}$$

where, A_{v0} is the active area available before poisoning and θ_{s} is the surface coverage of sulfur. When the surface is fully covered with sulfur, the active area becomes zero. Assuming surface diffusion to be negligible, the fractional surface coverage θ_k of various species is calculated from [21]

$$\frac{\mathrm{d}\theta_k}{\mathrm{d}t} = \frac{\sigma_k \dot{s}_k}{\Gamma}, \quad k = N_{\mathrm{g}} + 1, \ldots, N_{\mathrm{g}} + N_{\mathrm{s}}. \tag{6}$$

Here σ_k is the number of sites occupied by adsorbed species k, Γ is the total site density, $\dot{s}_k$ is the molar production rate of surface adsorbed species k, and N_{s} is the number of surface species. Calculation of $\dot{s}_k$ from an elementary like reaction mechanism is published in a number of previous articles [21, 22, 23]. Method of lines is applied to solve equations 1 and 6 simultaneously by using the ODE solver CVODE [24]. The entire model is implemented in C++.

3. Kinetic model

The detailed kinetic model developed for reforming of biogas on Ni is given in Table 1. The mechanism contains 68 reactions among 8 gasphase species, 17 surface adsorbed species, and the catalytic surface. While solving Eq. 6, the catalytic surface is also considered as a surface species. i.e., N_{s} includes the surface adsorbed species and the free catalytic surface. The adsorption of gas phase species on the catalytic surface is expressed as sticking reactions. It is generally well accepted that, H_2S chemisorbs dissociatively on Ni surface. However, there is no consensus on the number of Ni sites required for dissociative adsorption or the number of active sites that a sulfur atom may occupy. It is likely that at low temperature, the dissociative adsorption involves two Ni sites and at high temperature it involves only one Ni site. Although Rostrup-Nielsen [25] postulates the following scheme

$$\mathrm{H_2S(g) + Ni \rightleftharpoons Ni - S + H_2(g)} \tag{7}$$

for the adsorption of H_2S on Ni at high temperature, he does not make a final claim on this. Nevertheless, his data fitting to Langmuir isotherm leads to the conclusion that sulfur occupies only one site at high temperature. Since the mechanism developed here is for use at high temperature, sulfur is assumed to occupy only one site. Formation of bulk sulfide is not considered in this study as they form only at significantly high H_2S partial pressures [25]. For the disproportionation and recombination reactions the activation energies are calculated by applying UBI-QEP method[16], which requires the chemisorption energies and bond dissociation energies of various surface adsorbed and gas-phase species. Table 2 lists the chemisorption energies and bond dissociation energies of all the species involved in the reaction mechanism.

The pre-exponential factors are adjusted to reproduce the experimental observations and the entire mechanism is made thermodynamically consistent. One of the major problem in developing a thermodynamically consistent surface reaction mechanism is the non availability of thermochemistry data for the surface adsorbed species. The lack of thermochemistry data does not allow the calculation of equilibrium constant and hence the calculation of reverse reaction rate from equilibrium constant. Therefore, the forward and reverse reaction rates are defined with their own rate laws. However, the rate laws for every sin-

gle reaction must follow the thermodynamic rules

$$\Delta H_{\mathrm{r}} = E_{\mathrm{f}} - E_{\mathrm{r}}, \quad \text{and} \quad \frac{\Delta S_{\mathrm{r}}}{R} = \ln\left(\frac{A_{\mathrm{f}}}{A_{\mathrm{r}}}\right). \tag{8}$$

Here ΔH_{r} and ΔS_{r} are respectively the enthalpy change and entropy change for the reaction, E_{f} and E_{r} are respectively the enthalpy of the forward and reverse reactions, and A_{f} and A_{r} are respectively the forward and reverse reaction pre-exponential factors. A given reaction may contain gasphase species and/or surface adsorbed species. If only gas-phase specie are involved then there is no difficulty in ensuring the thermodynamic consistency due to the availability of thermochemistry data. When the reaction involves surface species whose thermochemistry is unknown, the free energy change for the reaction can be expressed in terms of linear combination of known and unknown free energies as

$$\Delta_i G_0 = \sum_{k=1}^{N_{\mathrm{u}}} \nu_{\mathrm{ki}} \tilde{G}_k^0(T) + \sum_{k=N_{\mathrm{u}}+1}^{N} \nu_{\mathrm{ki}} G_k^0(T). \tag{9}$$

Here $\Delta_i G_0$ is the free energy change for reaction i and ν_{ki} is the difference in stoichiometric coefficients of species k in the reactants and products. The free energy of species k can be evaluated in terms of polynomial coefficients according to

$$G_k^0 = a_{0,\mathrm{k}} + a_{1,\mathrm{k}} T + a_{2,\mathrm{k}} T^2 + a_{3,\mathrm{k}} T^3 + a_{4,\mathrm{k}} T^4 + a_{5,\mathrm{k}} T^5 + a_{6,\mathrm{k}} T \ln T. \tag{10}$$

The polynomial coefficients are known for all the gas-phase species. Eq 9 can be written for every single reaction in a mechanism, however, constrained by Eq. 8 and the unknown coefficients can then be calculated using a weighted least square method. We refer an interested reader to an earlier publication on this method [21].

4. Results and discussion

The kinetic model presented in Table 1 is developed by fine tuning the pre-exponential factors to reproduce our own experiments [27]. The only adjustable parameter in the modeling results presented below is A_{v0}. Throughout the simulation an initial specific surface area A_{v0}=18×10^4 m^{-1} is used at 973 K and A_{v0}=15×10^4 m^{-1} is used at 1073 K. The porosity is assumed to be 40% and the tortuosity is assumed to be 3.5 throughout the simulations. If any other value is used for a particular calculation that is explicitly stated in the text. To check the predictive capability of the mechanism we have simulated the experiments reported by other research groups [3, 17, 18] in addition to our own experiments.

4.1. Sensitivity Analysis

Sensitivity analysis is performed to elucidate the effect of various reaction parameters on sulfur coverage. In the analysis presented here, the sensitivity coefficients are defined as follows

$$\mathrm{SC} = \frac{\phi - \phi_0}{\phi_0}, \tag{11}$$

where

$$\phi = \frac{1}{\tau}\int_0^t \theta_{\mathrm{s}} dt, \quad \phi_0 = \frac{1}{\tau}\int_0^t \theta_{\mathrm{s}}^0 dt \tag{12}$$

Here ϕ is the total surface coverage of sulfur for ±5% change in pre-exponential factors and ϕ_0 is the total surface coverage of sulfur for pre-exponential factors as noted in Table 1. Figure 1 shows the scaled value of the sensitivity coefficient with respect to absolute maximum for major reactions that affect the formation of sulfur on Ni. The most sensitive reactions for the formation of adsorbed sulfur is the H_2S sticking reaction (R7) and H_2S desorption reaction (R45). An increase in sticking coefficient results in higher sulfur coverage, whereas an increase in H_2S desorption pre-exponential factor results in lower sulfur coverage. The sticking coefficient of H_2S is generally found be higher than 0.5 [26]. Therefore, in this mechanism we used a sticking coefficient of 0.6 for H_2S. In addition to these reactions, hydrogen abstraction reaction from H_2S and the reaction between adsorbed H_2S and O atom are also found to be influencing the formation of adsorbed sulfur. A positive change in R52 leads to the formation of SH, which further dissociates to give adsorbed sulfur. Since surface coverage of O facilitates the formation of SH from adsorbed H_2S through R52, a positive change in R16 also results in more adsorbed sulfur. Increasing the pre-exponential factor of R52 and R47 also results in faster deactivation.

4.2. Model predictions without sulfur poisoning

Comparison between model predictions and experimental observations made by Ashrafi et al. [3] for CH_4 and CO_2 conversions are shown respectively in Fig. 2(a) and Fig. 2(b). The experiments were performed in a fixed bed reactor with S/C ratio of ~2.7 and CH_4 to CO_2 ratio of 1.5. The reactor model described in section 2 is used for the simulations with A_{v0} = 6520×10^3 m^{-1}. The steady state model predictions for CH_4 conversions are in good agreement with the experimental observations and are well within the limits of equilibrium predictions. The equilibrium compositions are calculated using DETCHEM software [28]. Deviation from experimental observation is present only at low temperatures (873 K), which are not anyway practically useful for biogas reforming. As far as CO_2 conversions are concerned, the experimental observations violate thermodynamic predictions. Thermodynamics predicts the maximum possible conversion or yield. Although the experimentally observed CO_2 production (negative conversion in Fig. 2(b)) is within the thermodynamic limits, the observed conversions are above that predicted by thermodynamics. Nevertheless, the model predictions are well within the thermodynamic limit. The comparison between model predictions and experimental observation for CO selectivity and H_2 yield are shown respectively in Fig. 3(a) and Fig. 3(b). In both cases the model predictions are in very good agreement with the experimental observations. For the given S/C ratio CO_2

participates in the reforming reaction only at temperatures higher than 1050 K. However, at 1050 K CH_4 conversion is almost 97% and therefore, the CO_2 production below 1050 K is probably due to water gas shift reaction. When the temperature exceeds 1050 K, the H_2 yield starts decreasing and the CO_2 conversion becomes positive; this indicates the occurrence of reverse water gas shift reaction. The reverse water gas shift reaction at high temperature is also confirmed by the increasing CO selectivity (Fig.3(a)). Although not discussed here, we were also able to reproduce the experiments reported by Kolbitsch et al.[17]. For all these simulations CO and H atoms are found to be the major surface adsorbed species.

4.3. Model predictions with sulfur poisoning

Comparison between the model predicted and experimentally observed deactivation at 973 K and 1073 K is shown respectively, in Figs. 4 and 5. The initial inlet mixture to the reactor contains 12.5% CH_4, 8.4% CO_2, 25.2% H_2O and 53.9% N_2 and the gas hourly space velocity is 3.35×10^4 h^{-1}. H_2S (20 and 50 ppm) is introduced after 1 hr into the experiments during which the reactor reaches steady state operation. The experiments simulated in this work represent the catalyst activity loss in terms of drop in CH_4 conversion. The 6 cm long fixed bed reactor is simulated using the reactor model presented in section 2. At 973 K, the model very well captures the experimentally observed deactivation profile for 20 ppm H_2S in the feed gas, but an early deactivation for 50 ppm (Fig. 4). Nevertheless, the qualitative nature of the deactivation profile and steady state conversions are well predicted. At 1073 K, the model-predicted deactivation matches very well with the experimental observation (Fig. 5).

The product composition from the reactor exit (on dry basis) during deactivation of the catalyst for 20 ppm and 50 ppm H_2S in the feed gas at 973 K is shown respectively in Fig. 6 and Fig. 7. The model predictions are in excellent agreement with the experimental measurements. At steady state the product mixture mainly contains H_2, CO, CO_2 and N_2, however, N_2 mole fractions are not shown in the figure. As soon as H_2S is introduced, the mole fractions of H_2 and CO starts to decrease and CO_2 and CH_4 starts to increase. This means that CO_2 also participated in the reforming reactions for the S/C ratio employed here (S/C=2). Generally CO_2 does not participate in reforming reactions at high S/C ratio; however, this is temperature dependent. For instance at 1023 K, CO_2 participates in reforming reaction only at S/C ratio below 2.5 [17]. The product mole fractions on dry basis for 20 ppm H_2S at 1023 K are shown in Fig. 8. As observed at 973 K and 20 ppm, the mole fractions of H_2 and CO start to decrease after introducing H_2S. Due to 100% CH_4 conversion there is no significant difference in the steady state mole fractions of CO and H_2 before introducing H_2S compared to operation at 973 K. However, higher operating temperature is beneficial in maintaining catalytic activity. Unlike operating at 973 K, the catalytic activity is not fully compromised at 1073 K even with higher H_2S content in the feed gas (Fig. 5). This low degree of activity loss at high temperature is due to the exothermic nature of chemisorption reactions. This leads to higher CH_4 conversion and hence higher H_2 and CO mole fractions, after achieving the saturation sulfur coverage at 1073 K. However, at 1073 K there is a slight disagreement with the model predictions and experimental observation for the mole fractions of H_2 and CO_2 at steady state after poisoning. The model slightly under predicts H_2 and CO_2 at steady state. Similar behavior is observed for 50 ppm H_2S in the feed gas at 1073 K.

H_2O conversion at different temperatures and H_2S concentrations is shown in Fig. 9. Before introducing H_2S, the H_2O conversion is high at 973 K compared to 1073 K. The model predicts 46% conversion at 973 K and 42% at 1073 K. These predictions are in very good agreement with thermodynamic prediction of 46.3% and 42% respectively at 973 K and 1073 K. The H_2O conversions start to drop on introducing H_2S. Since the catalyst deactivation is faster for 50 ppm H_2S compared to 20 ppm H_2S in the feed gas, the steam conversion also follows the same trend.

The average fractional surface coverage of various surface adsorbed species and free surface along the length of the reactor as a function of time for 973 K and 1073 K with 20 ppm H_2S in the feed mixture is shown respectively in Fig. 10(a) and Fig. 10(b). The major surface adsorbed species before introducing H_2S into the feed are CO and H atoms and most of the surface remains open for adsorption. As soon as H_2S is introduced, sulfur starts to occupy most of the surface and the coverages of CO and H starts to decrease. After poisoning at 973 K, adsorbed sulfur occupies 92.0% of the surface with 4% open surface. CO and H atoms still remain as the other major species on the surface. The average fractional surface coverage of sulfur increases linearly and then reaches the steady state asymptotically. At 1073 K, sulfur occupies only 66% of the surface with 16% open surface. However along the length of the reactor, the poisoning is not uniform. Figures 11(a) and 11(b) shows the buildup of sulfur coverages at 973 K and 1073 K along the length of the reactor. At both temperatures, the poisoning occurs from inlet towards the exit of the reactor as time proceeds. In fact as the poisoning proceeds, the location of the methane reforming reaction moves downstream through the reactor length. This sort of wave behavior is typical for parallel poisoning [11].

The predictive capability of the model is further explored by simulating the deactivation experiments reported by Ashrafi et al. [18]. The simulations are again performed using the fixed bed reactor model with CH_4 to CO ratio of 1.5 and S/C ratio is of ~3.0. The specific surface area used in this case is A_{v0} = 5520×10^3 m^{-1}. Figure 12(a) shows the model predictions against the experimentally observed CH_4 conversions for two different H_2S concentrations (31 ppm and 108 ppm) in the feed gas for reactor operating at 1073 K. The model very well predicts the experimentally observed CH_4 conversion for 31 ppm H_2S. However, for the 108 ppm case, the CH_4 conversions are

over predicted. The model predicts 37% conversion, while the experimentally observed conversion is only 18%. This may be attributed to the inconsistencies in the reported experimental data. A careful examination of CH_4 conversions reported by Ashrafi et al. for 1073 K reveals some discrepancy in their data. In one case they report steady state CH_4 conversion of 32% at 1073 K with 145 ppm H_2S in the feed mixture. In another case they report 18% conversion for 108 ppm H_2S in the feed gas. These two are contradictory results, if 108 ppm H_2S results in 18% CH_4 conversion, then 145 ppm must result in a lower CH_4 conversion. Therefore, it is most likely that the the error is in the data reported at 108 ppm and in fact 108 ppm must result in higher CH_4 conversion, which is consistent with the predictions of the present model. At 1173 K, the model predictions are in good agreement with experimental observations. Figure 12(b) shows the comparison between the model predictions and the experimentally measured data. The model predicts 82% CH_4 conversion at 1173 K with 108 ppm H_2S in the feed gas, while the experimentally observed conversion is 86%. For 31 ppm, the model predicted conversion (91%) is very close the experimentally observed conversion of 93%. One may notice that the inlet composition used by Ashrafi et al. is different from the ones used in our own experiments. Thus, the model that is developed based on experiments conducted at one fixed composition, is able to predict catalyst deactivation at other conditions as well. Although the model predicts the deactivation profile for 108 ppm H_2S reported by Ashrafi et al. [18], it failed to predict the deactivation profiles with 100 ppm H_2S in the feed gas for our own experiments. At this stage, this appears to be due to diffusional effects coming into play at higher rates of poisoning at higher concentrations of H_2S. This requires further investigation. Therefore, we can say that the confidence interval for the model is 20 to 50 ppm H_2S in the feed gas for 973-1123 K. Finally the saturation coverages predicted by the model at different temperatures are shown Fig. 13. These linear trends are very much similar to the experimental observation by Nielsen et al. [29]. Although a direct comparison is not possible due to the difference in composition of the feed gas that is reported in dry basis, a qualitative agreement can be observed between the model predictions and experimental observations reported in [29]. The dry gas composition reported in [29] contains all the chemical species considered in this work. The authors report saturation sulfur coverages higher than 90% at 973 K for 50, 10 and 2 ppm H_2S in the feed gas, and our model also predicts saturation coverages higher than 90% at 973 K. Similar to the experiments, the model also predicts a linear decrease in sulfur coverage with increase in temperature.

5. Conclusions

A detailed kinetic model for simultaneous dry and steam reforming of biogas on Ni based catalyst is developed and validated against experimental data. The model can be used for simulating the reforming of biogas with and without H_2S. The catalyst deactivation is quantified in terms of loss in CH_4 conversion at different temperatures and H_2S concentrations. The model is developed by fine tuning the pre-exponential factors to reproduce the experimental observations. The entire mechanism is made thermodynamically consistent by using a previously published algorithm [21], which is briefly described in section 3. Brute force sensitivity analysis is carried out to understand the influence of various reaction parameters on the formation of sulfur. It is found that the sticking and desorption reactions of H_2S are the most influential ones. An increase in sticking coefficient and decrease in the pre-exponential factor for desorption reaction facilitates the formation of surface adsorbed sulfur. The only adjustable parameter used in the simulations is the surface area available per unit volume A_{v0}. The model is able to predict accurately the time on stream drop in CH_4 conversions and the product mole fractions at the reactor exit. Analysis of the fractional coverages along the reactor length reveals that during the initial stages of poisoning, the sulfur coverages are high near the reactor inlet. However, during the later stages, the surface coverage of sulfur increase towards the reactor exit. Since our experiments are conducted at one fixed composition the predictive capability of the kinetic model is further confirmed by simulating the experiments reported by Ashrafi et al. [18], which are performed for a different composition. In general the model is capable of predicting reforming of H_2S free biogas in the temperature range from 873-1200 K. However, the transients of deactivation are validated only in the temperature range of 973-1173 K and H_2S compositions from 20-50 ppm in the feed stream. Finally, although for a different composition, the model predicted saturation coverages are comparable to experimentally observed values.

Acknowledgment

We acknowledge the funding received from DST under the project SR/RC-UK/Fuel-Cell-03/2011/IITH (G)

References

[1] U. Izquierdo, V. Barrio, J. Requies, J. Cambra, M. Güemez, P. Arias, Int. J. Hydrogen Energy 38 (2013) 7623–7631.
[2] U. Izquierdo, V. Barrio, N. Lago, J. Requies, J. Cambra, M. Güemez, P. Arias, Int. J. Hydrogen Energy 37 (18) (2012) 13829–13842.
[3] M. Ashrafi, T. Pro, C. Pfeifer, H. Hofbauer, Energy Fuels 22 (15) (2008) 4182–4189.
[4] B. Schädel, M. Duisberg, O. Deutschmann, Catal. Today 142 (2009) 42–52.
[5] J. Oudar, Catal. Rev. Sci. Eng. 22 (1980) 171–195.
[6] C. H. Bartholomew, D. G. Weatherbee, G. A. Jarvi, J. Catal. 60 (1979) 257–269.
[7] L. Li, C. Howard, D. L. King, M. Gerber, R. Dagle, D. Stevens, Ind. Eng. Chem. Res. 49 (2010) 10144–10148.
[8] J. R. Rostrup-nielsen, J. Catal. 178 (1971) 171–178.
[9] C. H. Bartholomew, Appl. Catal., A 212 (2001) 17–60.
[10] P. Forzatti, L. Lietti, Catal. Today 52 (1999) 165–181.
[11] G. F. Froment, Appl. Catal., A 212 (2001) 117–128.
[12] L. Radovic, M. Vannice, Appl. Catal. 29 (1987) 1–20.
[13] G. A. Fuentes, Appl. Catal. 15 (1985) 33–40.
[14] P. L. Benito, A. G. Gayubo, T. Aguayo, M. Castilla, Ind. Eng. Chem. Res. 35 (1996) 81–89.
[15] V. M. Janardhanan, O. Deutschmann, J. Power Sources 162 (2006) 1192–1202.
[16] E. Shustorovich, Adv. Catal. 37 (1990) 101–163.
[17] P. Kolbitsch, C. Pfeifer, H. Hofbauer, Fuel 87 (2008) 701–706.
[18] M. Ashrafi, C. Pfeifer, T. Pro, H. Hofbauer, Energy Fuels 22 (2008) 4190–4195.
[19] R. B. Bird, W. E. Stewart, E. N. Lightfoot, Transport Phenomena, 2nd Edition, John Wiley & Sons, 2002.
[20] J. A. Moulijn, A. E. V. Diepen, F. Kapteijn, Appl. Catal., A 212 (2001) 3–16.
[21] S. Appari, V. M. Janardhanan, S. Jayanti, L. Maier, S. Tischer, O. Deutschmann, Chem. Eng. Sci. 66 (2011) 5184–5191.
[22] V. M. Janardhanan, O. Deutschmann, Z. Phys. Chem. 221 (2007) 443–478.
[23] V. M. Janardhanan, O. Deutschmann, Electrochim. Acta 56 (27) (2011) 9775–9782.
[24] A. Hindmarsh, P. Brown, K. Grant, S. Lee, R. Serban, D. Shumaker, C. Woodward, ACM Transactions on Mathematical Software 31 (2005) 363–396.
[25] J. R. Rostrup-Nielsel, J. Catal. 227 (1968) 220–227.
[26] R. I. Hegde, J. M. White, J. Phys. Chem. 90 (1986) 296–300.
[27] S. Appari, V. M. Janardhanan, R. Bauri, S. Jayanti, Int. J. Hydrogen Energy, http://dx.doi.org/10.1016/j.ijhydene.2013.10.056
[28] O. Deutschmann, S. Tischer, V. M. Janardhanan, C. Correa, D. Chatterjee, N. Mladenov, H. D. Minh, DETCHEM User manual (2007).
[29] J. R. Rostrup-nielsen, J. Hansen, S. Helveg, N. Christiansen, A.-K. Jannasch, Appl. Phys., A 430 (2006) 427–430.
[30] H. Sellers, E. Shustorovich, Surf. Sci., 346 (1996) 322–336.
[31] D. R. Huntley, O. Ridge, Surf. Sci., 240 (1990) 13–23.
[32] H. Sellers, E. Shustorovich, Surf. Sci., 356 (1996) 209–221.
[33] H. Sellers, E. Shustorovich, J. Mol. Catal., A 119 (96) (1997) 367–375.

Table 1: Detailed kinetic model for reforming of Biogas

R No	Reaction	A(cm,mol,s)	β	E_a [a]
R1	H_2 + (Ni) + (Ni) → H(Ni) + H(Ni)	0.01[b]	0	0
R2	O_2 +(Ni) +(Ni) → O(Ni) +O(Ni)	0.01[b]	0	0
R3	CH_4 +(Ni) → CH_4(Ni)	0.008[b]	0	0
R4	H_2O +(Ni) → H_2O(Ni)	0.1[b]	0	0
R5	CO_2 +(Ni) → CO_2(Ni)	1×10^{-05}[b]	0	0
R6	CO +(Ni) → CO(Ni)	0.5[b]	0	0
R7	H_2S +(Ni) → H_2 S(Ni)	0.6[b]	0	0
R8	SO_2 +(Ni) → SO_2(Ni)	0.02[b]	0	0
R9	H(Ni) +H(Ni) → (Ni) +(Ni) +H_2	2.676×10^{19}	0	81.40
R10	O(Ni) +O(Ni) → (Ni) +(Ni) +O_2	4.143×10^{23}	0	474.93
R11	CH_4(Ni) → (Ni) +CH_4	8.386×10^{15}	0	37.46
R12	H_2O(Ni) → (Ni) +H_2O	3.823×10^{12}	0	60.78
R13	CO_2(Ni) → (Ni) +CO_2	6.483×10^{07}	0	25.95
R14	CO(Ni) → (Ni) +CO	3.677×10^{11}	0	111.39
		$\epsilon_{CO(s)}$ [c]		-50
R15	O(Ni) +H(Ni) → OH(Ni) +(Ni)	5×10^{22}	0	97.90
R16	OH(Ni) +(Ni) → O(Ni) +H(Ni)	1.793×10^{21}	0	36.14
R17	OH(Ni) +H(Ni) → H_2O(Ni) +(Ni)	3×10^{20}	0	42.70
R18	H_2O(Ni) +(Ni) → OH(Ni) +H(Ni)	2.251×10^{21}	0	91.79
R19	OH(Ni) +OH(Ni) → O(Ni) +H_2O(Ni)	3×10^{21}	0	100.00
R20	O(Ni) +H_2O(Ni) → OH(Ni) +OH(Ni)	6.276×10^{23}	0	210.85
R21	O(Ni) +C(Ni) → CO(Ni) +(Ni)	5.2×10^{23}	0	148.10
R22	CO(Ni) +(Ni) → O(Ni) +C(Ni)	1.344×10^{22}	-3	116.06
		$\epsilon_{CO(s)}$ [c]		-50
R23	O(Ni) +CO(Ni) → CO_2(Ni) +(Ni)	2×10^{19}	0	123.60
		$\epsilon_{CO(s)}$ [c]		-50
R24	CO_2(Ni) +(Ni) → O(Ni) +CO(Ni)	4.627×10^{23}	-1	89.35
R25	HCO(Ni) +(Ni) → CO(Ni) +H(Ni)	3.7×10^{21}	0	0.00
		$\epsilon_{CO(s)}$ [c]		50
R26	CO(Ni) +H(Ni) → HCO(Ni) +(Ni)	3.903×10^{20}	-1	132.20
R27	HCO(Ni) +(Ni) → O(Ni) +CH(Ni)	3.7×10^{24}	-3	95.80
R28	O(Ni) +CH(Ni) → HCO(Ni) +(Ni)	4.741×10^{20}	0	110.00
R29	CH_4(Ni) +(Ni) → CH_3(Ni) +H(Ni)	3.7×10^{21}	0	57.70
R30	CH_3(Ni) +H(Ni) → CH_4(Ni) +(Ni)	5.903×10^{21}	0	61.51
R31	CH_3(Ni) +(Ni) → CH_2(Ni) +H(Ni)	3.7×10^{24}	0	100.00
R32	CH_2(Ni) +H(Ni) → CH_3(Ni) +(Ni)	1.265×10^{23}	0	55.26
R33	CH_2(Ni) +(Ni) → CH(Ni) +H(Ni)	3.7×10^{24}	0	97.10
R34	CH(Ni) +H(Ni) → CH_2(Ni) +(Ni)	4.001×10^{24}	0	79.11
R35	CH(Ni) +(Ni) → C(Ni) +H(Ni)	3.7×10^{21}	0	18.80
R36	C(Ni) +H(Ni) → CH(Ni) +(Ni)	4.529×10^{22}	0	161.06
R37	O(Ni) +CH_4(Ni) → CH_3(Ni) +OH(Ni)	1.7×10^{24}	0	88.30
R38	CH_3(Ni) +OH(Ni) → O(Ni) +CH_4(Ni)	9.728×10^{22}	0	30.35
R39	O(Ni) +CH_3(Ni) → CH_2(Ni) +OH(Ni)	3.7×10^{24}	0	130.10
R40	CH_2(Ni) +OH(Ni) → O(Ni) +CH_3(Ni)	4.538×10^{21}	0	23.60
R41	O(Ni) +CH_2(Ni) → CH(Ni) +OH(Ni)	3.7×10^{24}	0	126.80
R42	CH(Ni) +OH(Ni) → O(Ni) +CH_2(Ni)	1.435×10^{23}	0	47.05
R43	O(Ni) +CH(Ni) → C(Ni) +OH(Ni)	3.7×10^{21}	0	48.10
R44	C(Ni) +OH(Ni) → O(Ni) +CH(Ni)	1.624×10^{21}	0	128.60
R45	H_2S(Ni) → H_2S +(Ni)	1.108×10^{10}	-0.8	69.47

[a] Arrhenius parameters for the rate constants written in the form: k = AT^{β} exp(-E_a/RT) The units of A are given in terms of moles, centimeters, and seconds. E_a is in kJ/mol

[b] Sticking coefficient. Total available surface site density is $\Gamma=2.66\times10^{-9}$ mol/cm^2

[c] Coverage dependent activation energy

R46	SO_2(Ni) → SO_2 +(Ni)	2.709×10^{09}	0	102.50
R47	H_2S(Ni) +(Ni) → SH(Ni) +H(Ni)	5.5×10^{4}	1.2	29.31
R48	SH(Ni) +H(Ni) → H_2S(Ni) +(Ni)	1.291×10^{13}	0	106.19
R49	SH(Ni) +(Ni) → S(Ni) +H(Ni)	7.9×10^{11}	0	25.79
R50	S(Ni) +H(Ni) → SH(Ni) +(Ni)	6.375×10^{15}	0	142.94
R51	SH(Ni) +OH(Ni) → H_2S(Ni) +O(Ni)	1.053×10^{13}	0	29.72
R52	H_2S(Ni) +O(Ni) → SH(Ni) +OH(Ni)	8×10^{11}	-0.5	27.84
R53	S(Ni) +O(Ni) → SO(Ni) +(Ni)	1×10^{18}	1	296.82
R54	SO(Ni) +(Ni) → S(Ni) +O(Ni)	1.775×10^{12}	0	0.00
R55	SH(Ni) +O(Ni) → SO(Ni) +H(Ni)	1×10^{14}	-1	206.05
R56	SO(Ni) +H(Ni) → SH(Ni) +O(Ni)	2.115×10^{5}	0	0
R57	S(Ni) +OH(Ni) → SO(Ni) +H(Ni)	1×10^{21}	1	229.02
R58	SO(Ni) +H(Ni) → S(Ni) +OH(Ni)	3.352×10^{23}	-2.0	0.00
R59	SO_2(Ni) +(Ni) → SO(Ni) +O(Ni)	1×10^{18}	-0.5	106.31
R60	SO(Ni) +O(Ni) → SO_2(Ni) +(Ni)	9.029×10^{09}	1.5	0.00
R61	S(Ni) +H_2O(Ni) → SH(Ni) +OH(Ni)	1×10^{10}	0	143.37
R62	SH(Ni) +OH(Ni) → S(Ni) +H_2O(Ni)	1.652×10^{5}	0	0.00
R63	SH(Ni) +CO(Ni) → S(Ni) +HCO(Ni)	1.0×10^{4}	0	61.82
		$\epsilon_{CO(s)}$[c]		-50
R64	S(Ni) +HCO(Ni) → SH(Ni) +CO(Ni)	1.991×10^{12}	0	54.55
R65	SH(Ni) +CO(Ni) → SO(Ni) +CH(Ni)	1×10^{23}	0	223.41
		$\epsilon_{CO(s)}$[c]		-50
R66	SO(Ni) +CH(Ni) → SH(Ni) +CO(Ni)	3.066×10^{28}	0	0
R67	S(Ni) +CO(Ni) → SO(Ni) +C(Ni)	1×10^{13}	0	206.12
		$\epsilon_{CO(s)}$[c]		-50
R68	SO(Ni) +C(Ni) → S(Ni) +CO(Ni)	4.651×10^{15}	0	0

Table 2: Chemisorption (Q) and bond dissociation (D) energy of various surface adsorbed species [30, 31, 32, 33]

Species	Q (kcal mol^{-1})	D (kcal mol^{-1})
CH_4	6	398
CH_3	48	293
CH_2	83	183
CH	116	81
C	171	-
CO	27	257
CO_2	6	390
HCO	50	274
O	115	-
H	63	-
OH	61	102
H_2O	17	220
H_2S	19	173
SH	65	82
S	112	-
SO	17	125
SO_2	36	132

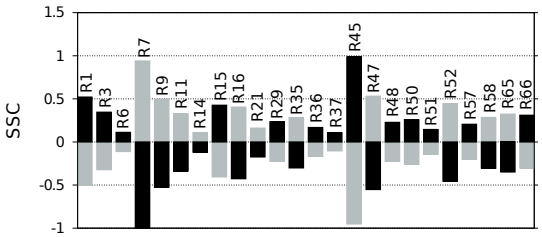

Figure 1: Scaled sensitivity of various reactions on sulfur coverage. Gray bars represent a 5% increase in the pre-exponential factors and black bars represent 5% decrease in pre-exponential factors.

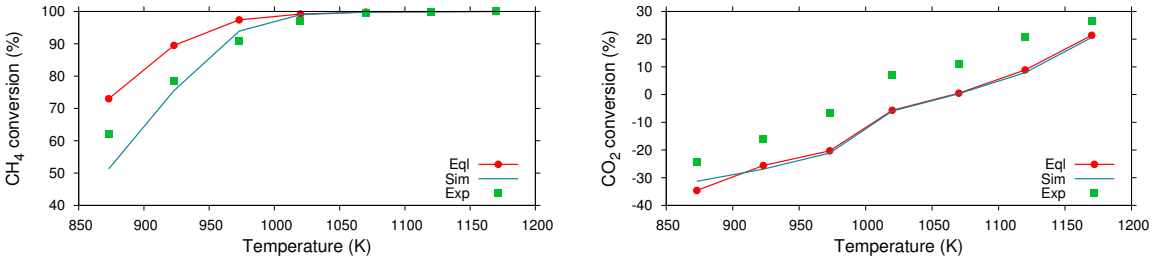

(a) CH_4 conversions as a function of temperature

(b) CO_2 conversions as a function of temperature

Figure 2: Comparison between experimental data (Exp), equilibrium predictions (Eql), and model predictions (Sim). The experimental data is from [3]. The S/C ratio employed is~2.7 and CH_4/CO_2 ratio is 1.5

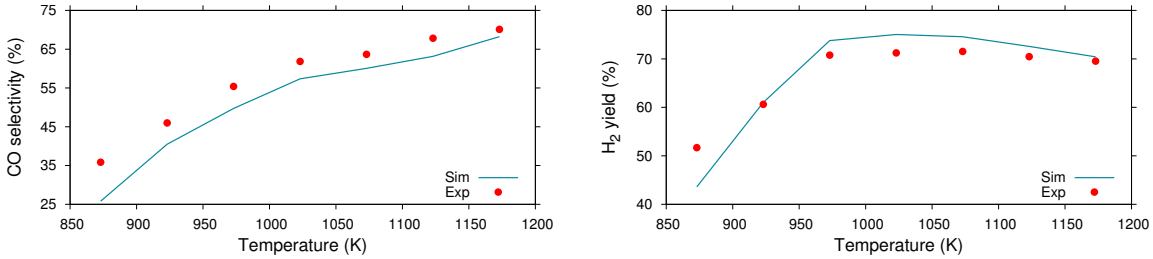

(a) CO selectivity as a function of temperature

(b) H_2 yield as a function of temperature

Figure 3: Comparison between experimental data (Exp) and model predictions (Sim). The experimental data is from [3]. The S/C ratio employed is~2.7 and CH_4/CO_2 ratio is 1.5

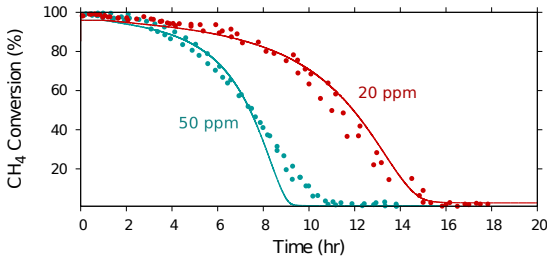

Figure 4: Comparison between the model predicted deactivation and experimental observations made at 973 K.

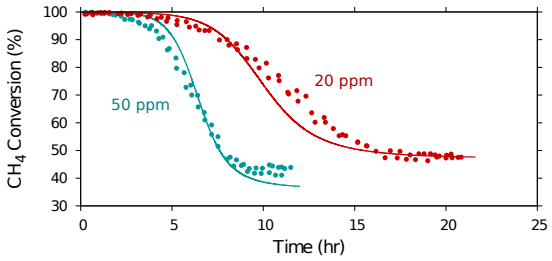

Figure 5: Comparison between the model predicted deactivation and experimental observations made at 1073 K.

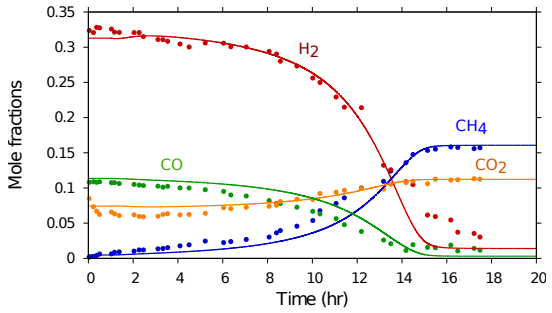

Figure 6: Comparison between the model predicted product composition during catalyst deactivation and experimental observations made at 973 K for 20 ppm H_2S in the feed.

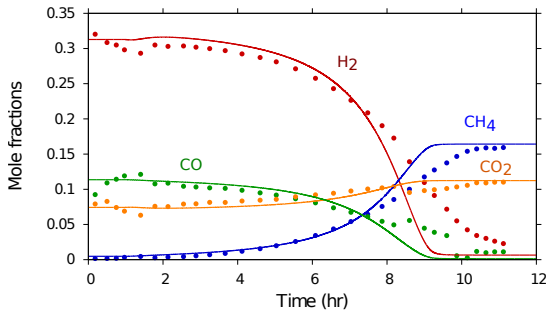

Figure 7: Comparison between the model predicted product composition during catalyst deactivation and experimental observations made at 973 K for 50 ppm H_2S in the feed.

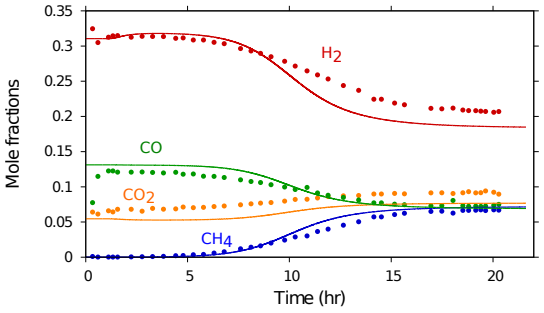

Figure 8: Comparison between the model predicted product composition during catalyst deactivation and experimental observations made at 1073 K for 20 ppm H_2S in the feed.

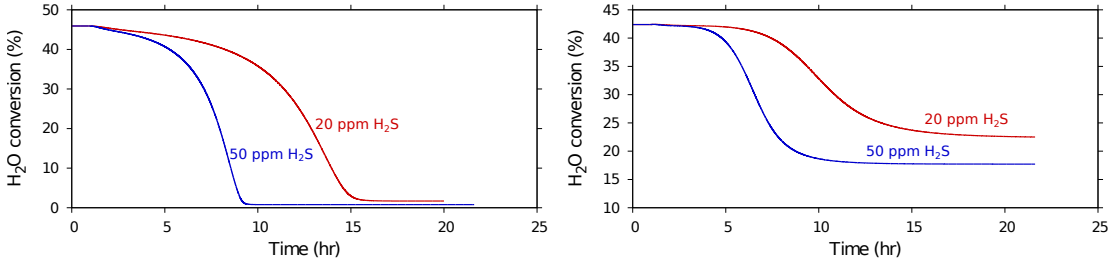

(a) H_2O conversions at 973 K

(b) H_2O conversions at 1073 K

Figure 9: H_2O conversions at 973 K and 1073 K with 20 and 50 ppm H_2S in biogas.

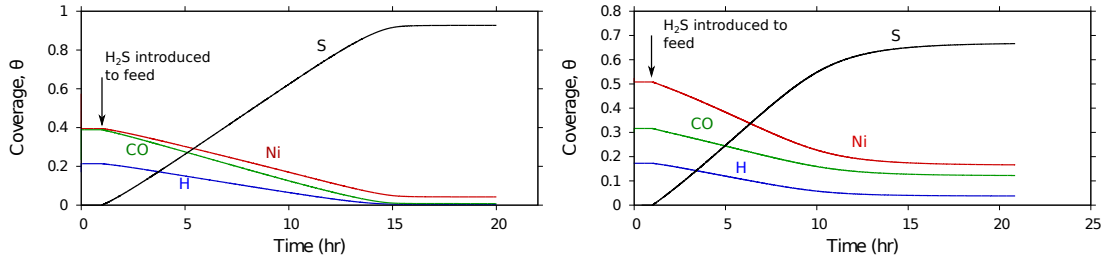

(a) Average fractional coverages at 973 K

(b) Average fractional coverage at 1073 K

Figure 10: Average fractional coverage along the length for major surface adsorbed species and the free coverage as a function of time at 973 K (10(a)) and 1073 K (10(b)). The inlet mixture contains 20 ppm H_2S.

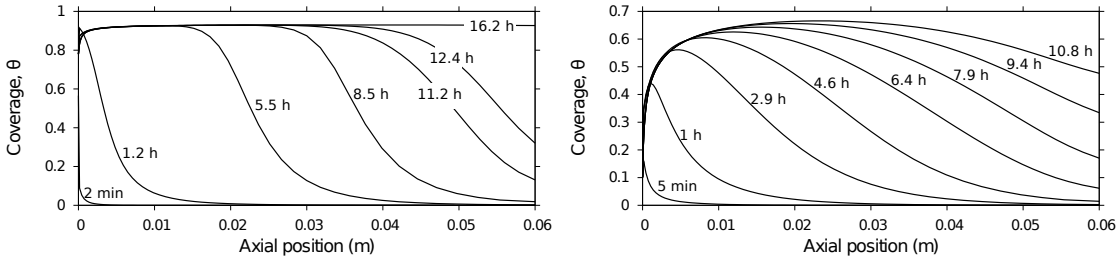

(a) Buildup of fractional coverage of sulfur at 973 K

(b) Buildup of fractional coverage of sulfur at 1073 K

Figure 11: Evolution of fractional coverage of sulfur on the catalyst surface for feed gas containing 20 ppm H_2 at 973 K and 1073 K.

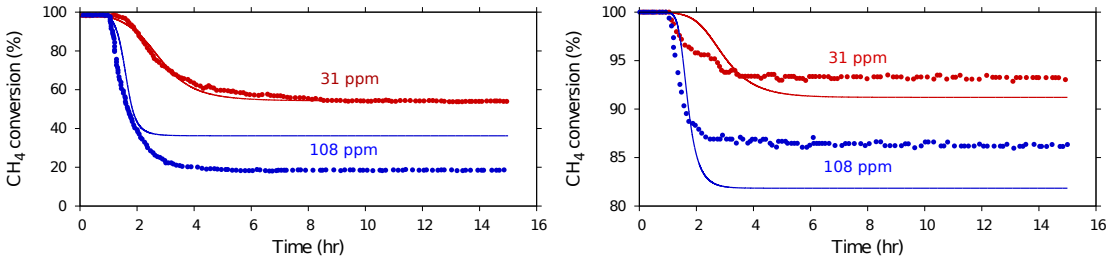

(a) CH_4 conversion at 1073 K (b) CH_4 conversion at 1173 K

Figure 12: Comparison between the model prediction and experimental observation for CH_4 conversion. Initial inlet mixture to the reactor contains CH_4 to CO_2 ratio of 1.5 and S/C ratio of ~3.

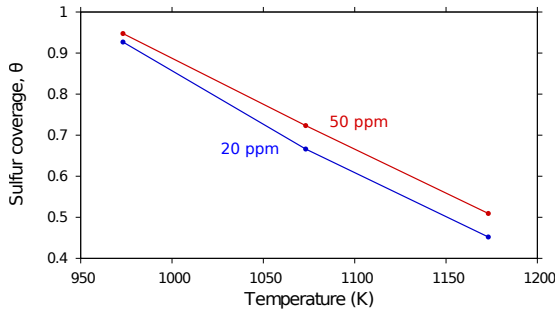

Figure 13: Model predicted saturation coverages at different temperatures.